electronic reprint

CRYSTALLOGRAPHIC COMMUNICATIONS

ISSN: 2056-9890

journals.iucr.org/e

Crystal structures and Hirshfeld surface analyses of (*N*-hexyl-*N*-methyldithiocarbamato-$\kappa^2 S,S'$)triphenyltin(IV) and [*N*-methyl-*N*-(2-phenylethyl)dithiocarbamato-$\kappa^2 S,S'$]triphenyltin(IV)

Rapidah Mohamad, Normah Awang, Nurul Farahana Kamaludin, Mukesh M. Jotani and Edward R. T. Tiekink

Acta Cryst. (2018). E**74**, 630–637

Acta Cryst E CRYSTALLOGRAPHIC COMMUNICATIONS

ISSN 2056-9890

Crystal structures and Hirshfeld surface analyses of (*N*-hexyl-*N*-methyldithiocarbamato-$\kappa^2 S,S'$)triphenyltin(IV) and [*N*-methyl-*N*-(2-phenylethyl)-dithiocarbamato-$\kappa^2 S,S'$]triphenyltin(IV)

Rapidah Mohamad,[a] Normah Awang,[b]‡ Nurul Farahana Kamaludin,[b] Mukesh M. Jotani[c] and Edward R. T. Tiekink[d]*

[a]Biomedical Science Programme, Faculty of Health Sciences, Universiti Kebangsaan Malaysia, Jalan Raja Muda Abdul Aziz, 50300 Kuala Lumpur, Malaysia, [b]Environmental Health and Industrial Safety Programme, Faculty of Health Sciences, Universiti Kebangsaan Malaysia, Jalan Raja Muda Abdul Aziz, 50300 Kuala Lumpur, Malaysia, [c]Department of Physics, Bhavan's Sheth R. A. College of Science, Ahmedabad, Gujarat 380001, India, and [d]Research Centre for Crystalline Materials, School of Science and Technology, Sunway University, 47500 Bandar Sunway, Selangor Darul Ehsan, Malaysia. *Correspondence e-mail: edwardt@sunway.edu.my

Received 26 March 2018
Accepted 30 March 2018

Edited by W. T. A. Harrison, University of Aberdeen, Scotland

‡ Additional correspondence author, e-mail: awang_normah@yahoo.com.

Keywords: crystal structure; organotin; dithiocarbamate; Hirshfeld surface analysis.

CCDC references: 1833664; 1833663

Supporting information: this article has supporting information at journals.iucr.org/e

The crystal and molecular structures of two triphenyltin dithiocarbamate compounds, *viz*. $[Sn(C_6H_5)_3(C_8H_{16}NS_2)]$, (I), and $[Sn(C_6H_5)_3(C_{10}H_{12}NS_2)]$, (II), are described. The dithiocarbamate ligand in each molecule coordinates in an asymmetric fashion resulting in heavily distorted tetrahedral C_3S coordination geometries for the Sn atoms, with the distortions traced to the close approach of the non-coordinating thione-S atom. The molecular packing in both compounds features C—H···π(Sn-phenyl) interactions. In (I), the donors are Sn-phenyl-C—H groups leading to centrosymmetric aggregates, while in (II), the donors are both Sn-phenyl-C—H and methyl-C—H groups leading to supramolecular chains propagating along the *b* axis. The identified aggregates assemble into their respective crystals with no directional interactions between them. An analysis of the Hirshfeld surfaces show distinctive patterns, but an overwhelming predominance (>99% in each case) of H···H, C···H/H···C and S···H/H···S contacts on the respective Hirshfeld surface.

1. Chemical context

A vast array of different dithiocarbamate anions, $^{-}S_2CNRR'$, has been prepared, which stems simply from the ability to alter the substituents in the starting amines used to prepare them. A key interest in dithiocarbamate compounds of both transition metals and main-group elements relates to their biological activity (Hogarth, 2012). Of particular relevance to the present study is the anti-microbial potential exhibited by organotin dithiocarbamates (Tiekink, 2008). In an on-going study of biological potential, organotin(IV) species have been complexed with two non-symmetric dithiocarbamate ligands, namely, with R = Me and R' = *n*-Hex and CH_2CH_2Ph. Previously, similar species, *i.e.* R = benzyl and R' = CH_2CH_2Ph (Mohamad, Awang, Kamaludin & Abu Bakar, 2016; Segovia *et al.*, 2002) and R = Me and R' = *n*-Bu (Segovia *et al.* 2002) have been tested for their toxicity using a bioassay based on the inhibition of the growth of *Escherichia coli* with the latter compound being most toxic according to the EC_{50} value measured *in vitro* (Segovia *et al.*, 2002). These results gave rise to the suggestion that increasing the length of the alkyl chain leads to enhanced solubility/activity of the compound

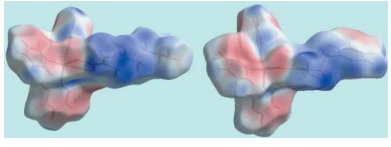

(Segovia *et al.*, 2002). Complementing these biological investigations (Mohamad, Awang, Kamaludin & Abu Bakar, 2016; Mohamad, Awang & Kamaludin, 2016) are structural studies of organotin dithiocarbamates (Mohamad, Awang, Jotani & Tiekink, 2016; Mohamad, Awang, Kamaludin, Jotani *et al.*, 2016; Mohamad *et al.*, 2017, 2018) and in continuation of the latter, herein, the crystal and molecular structures of $(C_6H_5)_3Sn[S_2CN(Me)Hex]$ (I) and $(C_6H_5)_3Sn[S_2CN(CH_3)CH_2CH_2Ph]$ (II) are reported along with a Hirshfeld surface analysis to provide more details on the molecular packing.

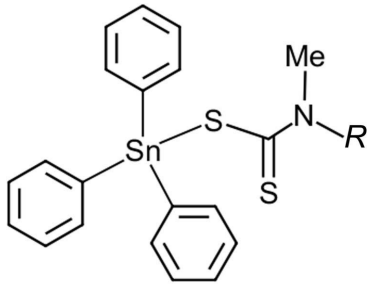

(I) *R* = *n*-Hex
(II) *R* = CH_2CH_2Ph

2. Structural commentary

The tin atom in (I), Fig. 1*a*, is coordinated by three *ipso*-carbon atoms along with a dithiocarbamate ligand. As seen from Table 1, the dithiocarbamate ligand forms quite disparate Sn—S1, S2 bond lengths, with Δ(Sn—S) = (Sn—S_{long} – Sn—S_{short}) being 0.64 Å. This asymmetry is confirmed in the differences in the C—S bond lengths with the C1—S1 bond associated with the short Sn—S1 contact, at 1.761 (4) Å, being significantly longer than the C1—S2 bond, *i.e.* 1.688 (4) Å, involving the weakly bound S2 atom. If the S2 atom is ignored, the coordination geometry about the tin atom is distorted C_3S tetrahedral with the range of angles being 90.00 (11)°, for S1—Sn—C31, to 121.53 (10)°, for S1—Sn—C11. The wide angle clearly reflects the influence of the close approach of the S2 atom, Fig. 1*a* and Table 1. If the S2 atom is considered a significant bonding interaction, the resultant C_3S_2 donor set is almost perfectly intermediate between ideal square-pyramidal (SP) and trigonal–bipyramidal (TP). This is quantified in the value of τ = 0.52, which compares with the ideal values for SP and TP geometries of τ = 0.0 and 1.0, respectively (Addison *et al.*, 1984). In the latter description, the range of angles is wide with the S1—Sn—S2 chelate angle being acute [63.26 (3)°] and with the widest angle [152.54 (11)°] being for S2—Sn—C31. The *n*-hexyl chain is linear up to the terminal methyl group. Thus, the N1—C3—C4—C5, C3—C4—C5—C6 and C4—C5—C6—C7 torsion angles of 175.9 (4), 178.5 (4) and 178.9 (5)°, respectively, indicate + anti-periplanar descriptors but, that of C5—C6—C7—C8, *i.e.* −66.4 (8)°, indicative of a − syn-clinal disposition.

The molecular structure of (II), Fig. 1*b*, resembles closely that described for (I). Indeed, a comparison of the key bond lengths included in Table 1 show there are no chemically significant differences between the common parts of the molecules. In terms of bond angles, for a tetrahedral description, the range of angles in (II) is smaller, by 2°, than in (I), again, not chemically significant. If the five-coordinate C_3S_2 description pertains, the value of τ = 0.60 indicates a distortion towards TP. The phenylethyl chain is kinked as seen in the N1—C3—C4—C5 and C3—C4—C5—C6 torsion angles of −175.8 (3) and 91.9 (5)°, respectively.

Table 1
Selected interatomic parameters (Å, °) for (I) and (II).

Parameter	(I)	(II)
Sn—S1	2.4672 (11)	2.4636 (9)
Sn···S2	3.1113 (11)	3.1066 (10)
C1—S1	1.761 (4)	1.761 (4)
C1—S2	1.688 (4)	1.678 (4)
C1—N1	1.330 (5)	1.342 (5)
S1—Sn···S2	63.26 (3)	63.42 (3)
S1—Sn···C11	121.53 (10)	111.30 (9)
S1—Sn···C31	90.00 (11)	92.68 (9)
C11—Sn—C21	114.88 (15)	119.27 (13)
S2—Sn···C31	152.54 (11)	155.43 (9)

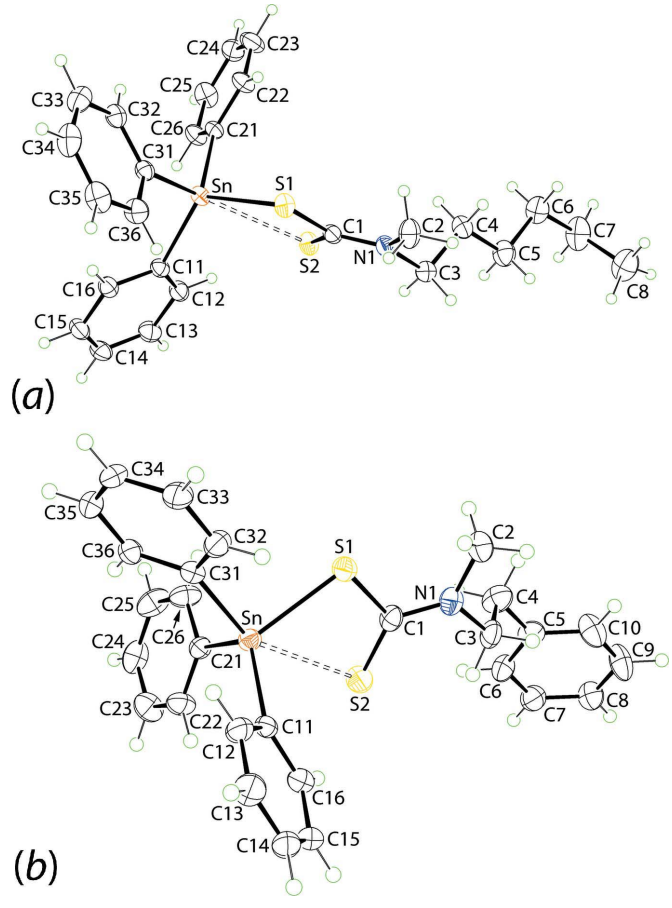

Figure 1
The molecular structures of (*a*) (I) and (*b*) (II), showing the atom-labelling schemes and displacement ellipsoids at the 50% probability level.

Table 2
Hydrogen-bond geometry (Å, °) for (I).

*Cg*1 and *Cg*2 are the centroids of the (C11–C16) and (C31–C36) rings, respectively.

D—H···*A*	*D*—H	H···*A*	*D*···*A*	*D*—H···*A*
C32—H32···*Cg*1^{i}	0.95	2.88	3.630 (4)	137
C26—H26···*Cg*2^{i}	0.95	2.99	3.641 (5)	127

Symmetry code: (i) $-x+1, -y+1, -z$.

Table 3
Hydrogen-bond geometry (Å, °) for (II).

*Cg*1 and *Cg*2 are the ring centroids of the (C11–C16) and (C31–C36) rings, respectively.

D—H···*A*	*D*—H	H···*A*	*D*···*A*	*D*—H···*A*
C2—H2*B*···*Cg*1^{i}	0.98	2.99	3.779 (5)	138
C14—H14···*Cg*2^{ii}	0.95	2.95	3.754 (5)	143

Symmetry codes: (i) $-x+2, -y, -z+2$; (ii) $x, y-1, z$.

3. Supramolecular features

Tables 2 and 3 list the geometric parameters characterizing the intermolecular interactions operating in the crystals of (I) and (II), respectively. The molecular packing of (I) features centrosymmetric dimeric aggregates sustained by four phenyl-C—H···π(phenyl) interactions whereby all of the participating groups are derived from Sn-bound phenyl rings, Fig. 2*a*. Such cooperative C—H···π(phenyl) embraces have been described for many phenyl-rich systems and in instances

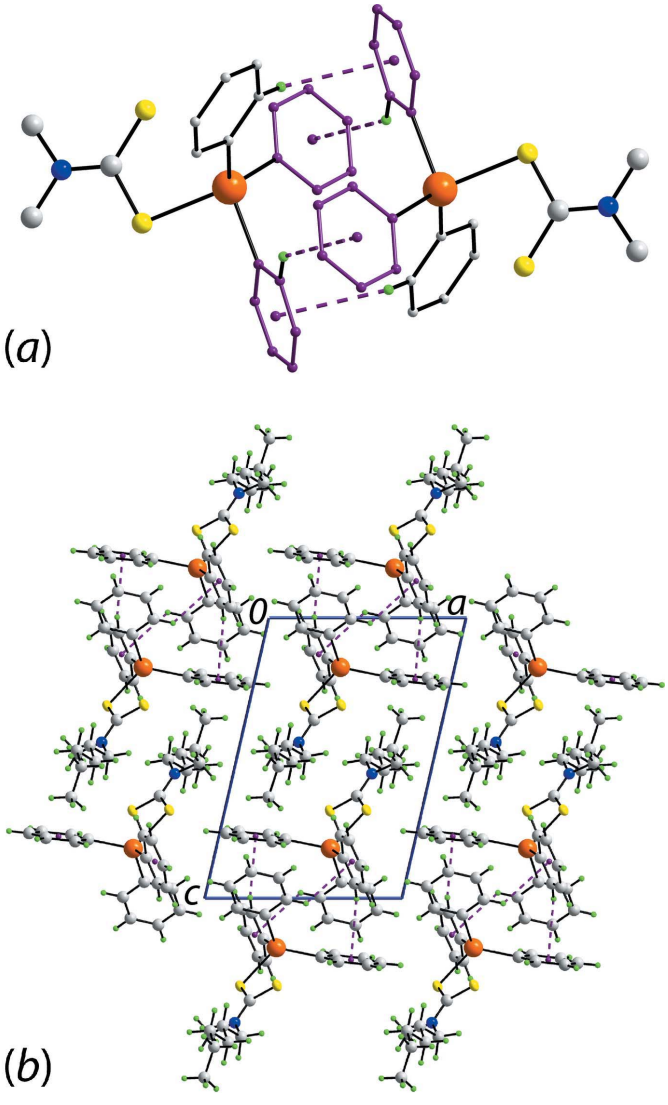

Figure 2
Molecular packing in the crystal of (I): (*a*) supramolecular dimer sustained by a four-fold embrace of phenyl-C—H···π(phenyl) interactions shown as purple dashed lines (for clarity, the phenyl rings are shown as small spheres, the interacting phenyl rings are highlighted in purple and only the N-bound carbon atoms of the dithiocarbamate substituents are shown) and (*b*) a view of the unit-cell contents shown in projection down the *b* axis.

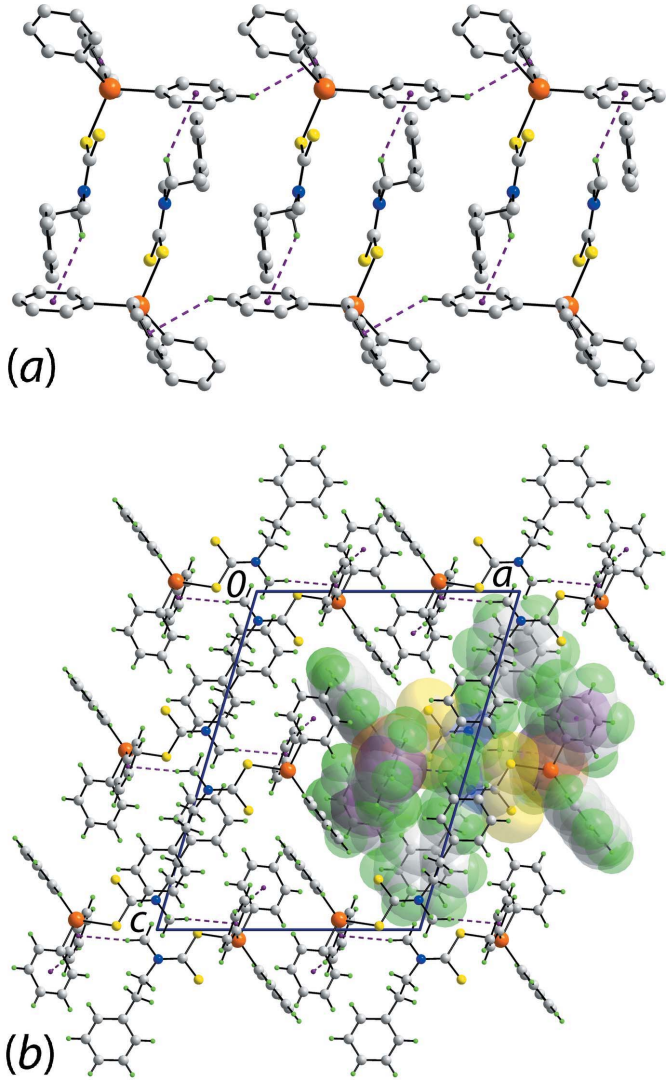

Figure 3
Molecular packing in the crystal of (II): (*a*) supramolecular chain sustained by C—H···π(phenyl) interactions shown as purple dashed lines and (*b*) a view of the unit-cell contents in projection down the *b* axis. One chain is highlighted in space-filling mode.

where six phenyl rings of two residues associate by edge-to-face interactions, *i.e.* a six-fold embrace, the energies of stabilization can resemble or even exceed that provided by strong conventional hydrogen bonding (Dance & Scudder, 2009). The supramolecular dimers stack parallel to the *b* axis with no directional interactions between successive aggregates. Globally, columns pack into layers in the *ab* plane. The layers inter-digitate along the *c* axis, again without specific interactions between proximate residues, Fig. 2*b*.

The molecular packing of (II) again features C—H···π interactions, as for (I), but with both methyl-H and Sn-bound-H hydrogen atoms as donors; the Sn-phenyl rings function as acceptors. As illustrated in Fig. 3*a*, the C—H···π interactions sustain a supramolecular chain aligned along the *b* axis. The chains pack into the three-dimensional architecture without directional interactions between then, Fig. 3*b*. As may be seen from Fig. 3*b*, centrosymmetrically related Ph_3Sn residues approach each other so as to form phenyl-embrace interactions as found in the molecular packing of (I), but none of the putative contacts are within the standard distance criteria assumed in *PLATON* (Spek, 2009).

4. Hirshfeld surface analysis

The Hirshfeld surface calculations for the triphenyltin dithiocarbamate derivatives (I) and (II) were performed in accord with recent work on related organotin dithiocarbamates (Mohamad *et al.*, 2017). Despite the similarity in composition, the structures of (I) and (II) exhibit different intermolecular environments because of the presence of different substituents in the respective dithiocarbamate ligands, *i.e.* *n*-hexyl in the former and phenylethyl in the latter.

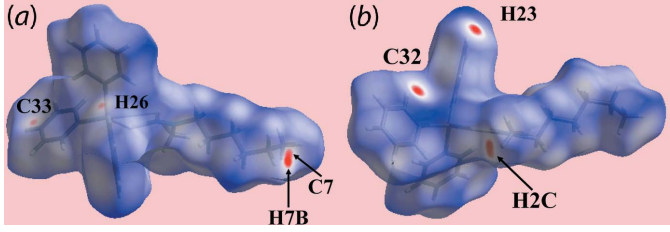

Figure 4
Views of Hirshfeld surface for (I) mapped over d_{norm} in the range −0.133 to +1.538 au.

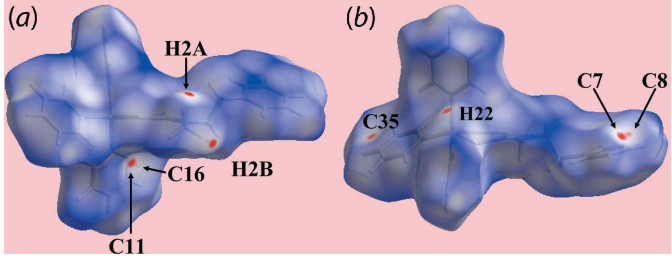

Figure 5
Views of Hirshfeld surface for (II) mapped over d_{norm} in the range −0.075 to +1.363 au.

Table 4
Summary of short interatomic contacts (Å) in (I) and (II).

Contact	Distance	Symmetry operation
(I)		
H2*C*···H7*B*	1.98	$x, -1+y, z$
H2*C*···C7	2.67	$x, -1+y, z$
H23···C32	2.57	$-x, -1+y, -1+z$
H26···C33	2.70	$1-x, -1-y, -z$
(II)		
H2*A*···H7	2.26	$2-x, \frac{1}{2}+y, \frac{3}{2}+z$
H9···H23	2.29	$1+x, y, z$
H2*A*···C7	2.68	$2-x, \frac{1}{2}+y, \frac{3}{2}+z$
H2*A*···C8	2.74	$2-x, \frac{1}{2}+y, \frac{3}{2}+z$
H2*B*···C11	2.70	$2-x, -y, 2-z$
H2*B*···C16	2.77	$2-x, -y, 2-z$
H22···C35	2.69	$1-x, -y, 2-z$

These differences are readily discerned from the differently shaped Hirshfeld surfaces mapped over d_{norm} for (I), Fig. 4, and (II), Fig. 5, which reflect the influence of short interatomic H···H and C···H/H···C contacts, Table 4, and comparatively weak C—H···π interactions, Tables 2 and 3.

The faint-red spots near the phenyl-C33 and H26 atoms in Fig. 4*a* reflect the presence of a weak C—H···π interaction, as summarized in Table 4. In both images of Fig. 4, the bright-red spots appearing near Sn-bound phenyl atoms C32 and H23, methyl-H2*C* and *n*-hexyl atoms C7 and H7*B* are indicative of the short interatomic H···H and C···H/H···C contacts involving these atoms, as listed in Table 4. The presence of similar intermolecular interactions in the crystal of (II) *cf.* (I), but involving different atoms, is also characterized by bright and faint-red spots on the Hirshfeld surfaces mapped over d_{norm} in Fig. 5. Thus, the C—H···π interaction is seen from the presence of bright-red spots near methyl-H2*B* and phenyl-C11 together with the pair of faint-red spots near the methyl-H2*B* and phenyl-C16 atoms in Fig. 5*a*. The influence of other short interatomic C···H/H···C contacts summarized in Table 4 are viewed as diminutive and faint-red spots near the respective atoms in Fig. 5*a*,*b*. The involvement of different atoms in the intermolecular interactions in the crystals of (I) and (II) is also confirmed from the views of their Hirshfeld surfaces mapped over electrostatic potential, Fig. 6, through the appearance of blue and red regions corresponding to positive and negative

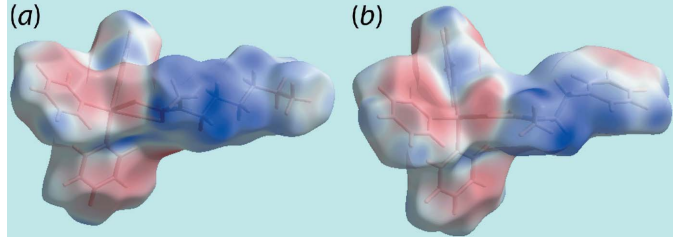

Figure 6
Views of Hirshfeld surface mapped over the electrostatic potential (the red and blue regions represent negative and positive electrostatic potentials, respectively) for a molecule of: (*a*) (I) in the range ±0.041 au and (*b*) (II) in the range −0.033 to +0.049 au.

Table 5
Percentage contributions of interatomic contacts to the Hirshfeld surface for (I) and (II).

Contact	Percentage contribution	
	(I)	(II)
H···H	66.1	57.8
C···H/H···C	25.6	33.7
S···H/H···S	7.6	7.6
N···H/H···N	0.4	0.6
C···N/N···C	0.2	0.0
S···N/N···S	0.1	0.0
C···S/S···C	0.0	0.3

electrostatic potentials around them. The different molecular environments about respective reference molecules are highlighted in Fig. 7.

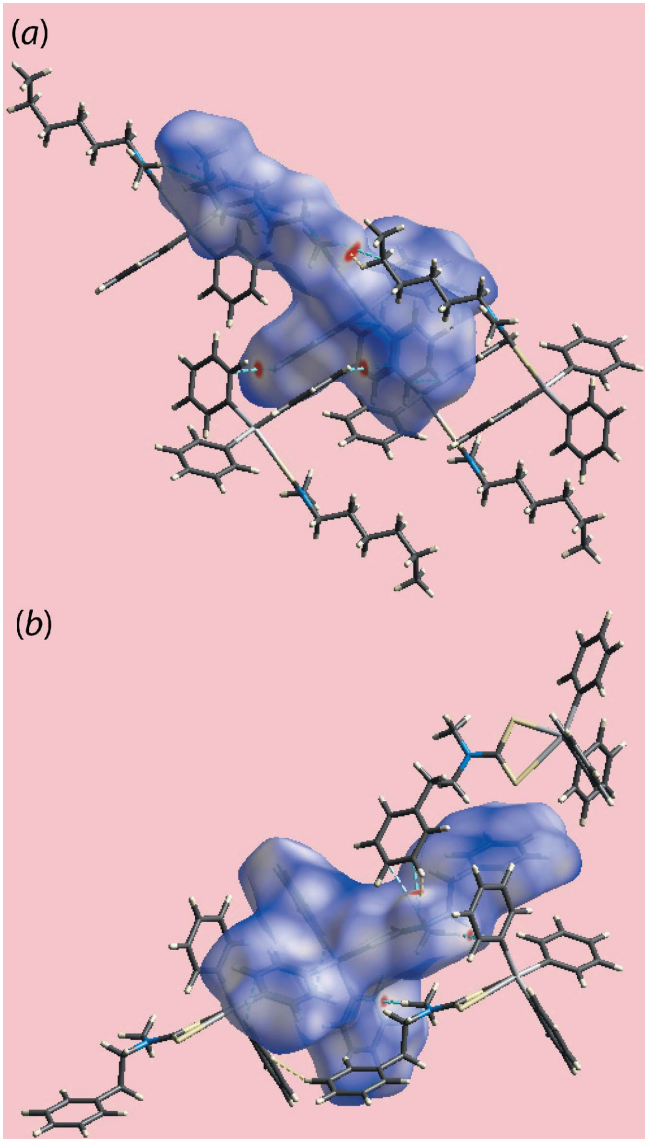

Figure 7
The immediate environment around reference molecules within d_{norm}-mapped Hirshfeld surfaces for (*a*) (I) and (*b*) (II), highlighting short interatomic H···H and C···H/H···C contacts by yellow and blue dashed lines, respectively

The distinct distribution of points in the overall two-dimensional fingerprint plots for (I) and (II), Fig. 8*a*, also highlight the different molecular environments for the two molecules. The significant contributions from H···H, C···H/H···C and S···H/H···S contacts to the Hirshfeld surfaces of both (I) and (II) are evident from Table 5. The short interatomic H···H contact between the methyl-H2*C* and *n*-hexyl-H7*B* atoms in (I) is viewed as a pair of closely spaced overlapping peaks with their tips at $d_e + d_i$ ~2.0 Å in the delineated plot (McKinnon *et al.*, 2007) Fig. 8*b*. A pair of well separated short peaks at $d_e + d_i$ ~2.2 Å observed in the corresponding fingerprint plot for (II) are due to the involvement of methyl-H2*A* and phenyl-H7, H9 and H23 atoms in comparatively weaker short interatomic H···H contacts, Table 4. The pair of very thin and long forceps-like tips at $d_e + d_i$ ~2.6 Å in the fingerprint plot delineated into C···H/H···C contacts for (I), Fig. 8*c*, is the result of a short interatomic contact between

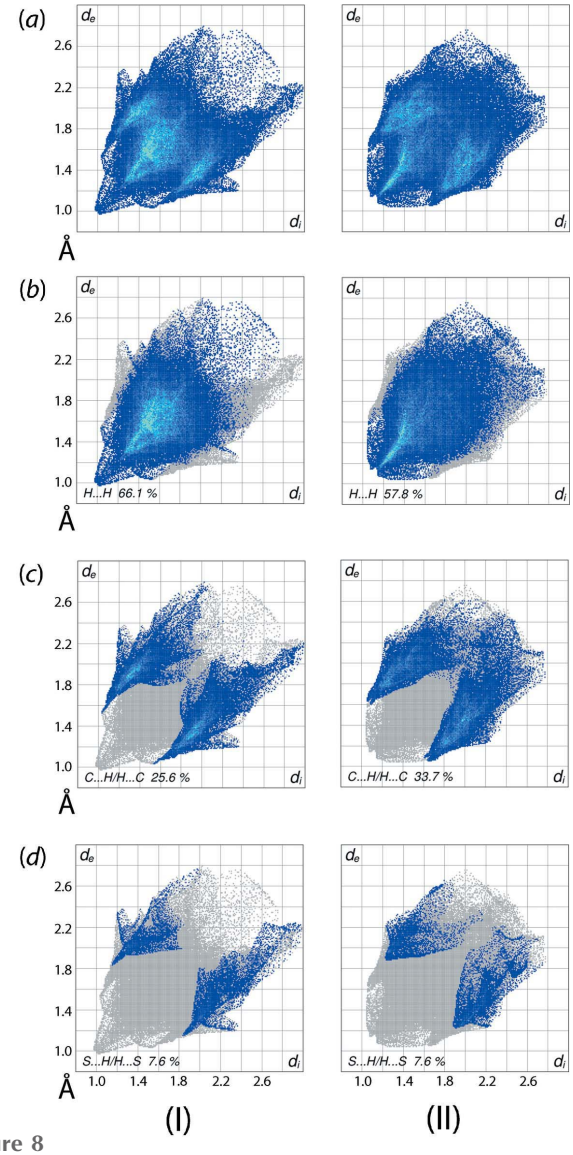

Figure 8
A comparison of the (*a*) full two-dimensional fingerprint plots for (I) and (II), and the plots delineated into (*b*) H···H, (*c*) C···H/H···C and (*d*) S···H/H···S contacts.

Table 6
Selected interatomic parameters (Å) for $Ph_3Sn(S_2CNRR')$.

Compound	R	R'	Sn—S_{short}	Sn—S_{long}	Δ(Sn—S)	Reference
(III)	Et	Et	2.429 (3)	3.096 (3)	0.67	Hook *et al.* (1994)
(IV)[a]	$(CH_2CH_2)_2C(H)CH_2CH_2$	$(CH_2CH_2)_2C(H)CH_2$	2.521 (3)	2.919 (3)	0.40	Ali *et al.* (2014)
			2.4735 (10)	2.9468 (10)	0.47	
(V)	CH_2Ph	CH_2CH_2Ph	2.4885 (5)	2.9120 (5)	0.42	Mohamad, Awang, Kamaludin, Jotani *et al.* (2016)
(VI)[b]	CH_2(3-pyridyl)	CH_2(3-pyridyl)	2.5165 (19)	3.2209 (19)	0.71	Gupta *et al.* (2015)
			2.4685 (19)	3.0397 (19)	0.57	

Notes: (*a*) non-symmetric binuclear molecule; (*b*) two independent molecules in the asymmetric unit.

phenyl-C32 and -H23 atoms while the points corresponding to other short interatomic contacts are merged within the plot. The presence of a pair of twin forceps-like tips at $d_e + d_i \sim 2.7$ Å in the C···H/H···C delineated plot for (II), Fig. 8*c*, also indicates the involvement of methyl-H2*A* and -H2*B*, and phenyl-C7, -C8, -C11, -C16 and -C35 atoms in short interatomic contacts, Table 4. Further, it is clear from the fingerprint plots delineated into S···H/H···S contacts, Fig. 8*d*, that the pair of spikes at $d_e + d_i \sim 3.0$ Å for (I) show van der Waals contacts whereas the pair of peaks at $d_e + d_i > 3.1$ Å for (II) show contacts farther than van der Waals separation. The other interatomic contacts summarized in Table 5 make a negligible contribution to their Hirshfeld surfaces.

5. Database survey

The dithiocarbamate ligands reported in the present study are quite rare, despite the rather large number of crystal structures of dithiocarbamate ligands available in the crystallographic literature (Groom *et al.*, 2016). Thus, the *N*-hexyl-*N*-methyldithiocarbamate ligand reported in (I), *i.e.* dtcI, has been reported in the crystal structures of $Ph_2Sn(dtcI)_2$ (Ramasamy *et al.*, 2013), $In(dtcI)_3$ (Park *et al.*, 2003), and in $Bi(dtcI)_3$ and its 1:1 1,10-phenanthroline adduct (Monteiro *et al.*, 2001). The uniform motivation for these studies was for their evaluation as useful precursors for the deposition of heavy element sulfide nanomaterials. In terms of the molecular structures, no special features in the mode of coordination are noted in the tin (Tiekink, 2008), indium (Heard, 2005) and bismuth (Lai & Tiekink, 2007) compounds. The *N*-methyl-*N*-phenylethyldithiocarbamate ligand, *i.e.* dtcII, has been reported only in its binary mercury(II) compound, *i.e.* $Hg(dtcII)_3$ (Green *et al.*, 2004), and again, its study was motivated by the desire to generate *β*–HgS thin films and its structure confirms to expectation (Jotani *et al.*, 2016).

Reflecting the interest in organotin dithiocarbamates, including their biological activity, there are over 50 structures of general formula $Ph_3Sn(S_2CNRR')$ in the Cambridge Structural Database (Groom *et al.*, 2016). Of these, seven are binuclear and are better represented as Ph_3SnS_2CN–*R*–NCS_2SnPh_3. In all, there are 56 independent coordination geometries and all conform to the same structural motif as described above for (I) and (II). The average Sn—S_{short} bond length is 2.47 Å and the average Sn—S_{long} bond length is 3.04 Å. This gives rise to an average Δ(Sn—S) of 0.57 Å. These values indicate the structures of (I) and (II) are outliers in that the values of Sn—S_{long} are generally longer than usually observed. An analysis of the available crystallographic data showed the shortest Sn—S1 bond length occurred in the structure of $Ph_3Sn(S_2CNEt_2)$ [(III); Hook *et al.* 1994] while the longest was found for one of the independent tin centres in binuclear $Ph_3Sn[S_2CN(CH_2CH_2)_2C(H)(CH_2)_3C(H)(CH_2CH_2)_2NCS_2]SnPh_3$ [(IV); Ali *et al.*, 2014], *i.e.* spanning the range 2.43 to 2.52 Å, Table 6. The shortest and longest of the Sn···S2 separations were found in $Ph_3Sn[S_2CN(CH_2Ph)CH_2CH_2Ph]$ [(V); Mohamad, Awang, Kamaludin, Jotani *et al.*, 2016] and for one of the two independent molecules of $Ph_3Sn\{S_2CN[CH_2(3\text{-pyridyl})]_2\}$ [(VI); Gupta *et al.*, 2015], *i.e.* spanning the range 2.91 to 3.22 Å, Table 6. The lack of systematic variations in these structural parameters is borne out by the disparity of the cited bonds with the second tin centre of non-symmetric (IV) and the second independent molecule of (VI). Thus, the range of Δ(Sn—S) for all structures was 0.40 to 0.74, with the correlation coefficient from the plot of Sn—S_{short} *versus* Sn—S_{long} being 0.52. Such a lack of correlation has often been noted in the structural chemistry of organotin dithiocarbamates and has been ascribed to the dictates of the molecular packing (Buntine *et al.*, 1998; Tiekink *et al.*, 1999; Muthalib *et al.*, 2014).

6. Synthesis and crystallization

All chemicals and solvents were used as purchased. The melting points were determined using an automated melting-point apparatus (MPA 120 EZ-Melt). C, H, N and S analyses were performed on a Leco CHNS-932 Elemental Analyzer. The IR spectra were obtained on a Perkin Elmer Spectrum GX from 4000 to 400 cm^{-1}. NMR spectra were recorded in $CDCl_3$ at room temperature on a Bruker AVANCE 400 111 HD.

Synthesis of triphenyltin(IV) *N*-hexyl-*N*-methyldithiocarbamate (I): *N*-hexyl-*N*-methylamine (Aldrich; 1.52 ml, 10 mmol) dissolved in ethanol (30 ml) was stirred at 277 K before a cold ethanolic solution of carbon disulfide (0.6 ml, 10 mmol) was added dropwise. The resulting mixture was stirred for 2 h. Then, triphenyltin(IV) chloride (Merck; 3.85 g, 10 mmol) dissolved in ethanol (25 ml) was added dropwise into the solution and stirring was continued for 2 h. The precipitate formed was filtered, washed with cold ethanol and dried. Recrystallization was achieved by dissolving the compound in a chloroform and ethanol mixture (1:1 *v*/*v*). This solution was allowed to slowly evaporate at room temperature

Table 7
Experimental details.

	(I)	(II)
Crystal data		
Chemical formula	$[Sn(C_6H_5)_3(C_8H_{16}NS_2)]$	$[Sn(C_6H_5)_3(C_{10}H_{12}NS_2)]$
M_r	540.38	560.37
Crystal system, space group	Triclinic, $P\overline{1}$	Monoclinic, $P2_1/c$
Temperature (K)	173	173
a, b, c (Å)	9.8590 (6), 10.4256 (5), 14.3960 (8)	14.3682 (4), 9.4758 (2), 19.2747 (6)
α, β, γ (°)	110.557 (5), 94.057 (5), 110.730 (5)	90, 106.450 (3), 90
V (Å^3)	1263.24 (13)	2516.84 (12)
Z	2	4
Radiation type	Cu $K\alpha$	Cu $K\alpha$
μ (mm^{-1})	9.67	9.73
Crystal size (mm)	0.30 × 0.20 × 0.05	0.10 × 0.10 × 0.05
Data collection		
Diffractometer	Agilent Technologies SuperNova Dual diffractometer with Atlas detector	Agilent Technologies SuperNova Dual diffractometer with Atlas detector
Absorption correction	Multi-scan (*CrysAlis PRO*; Agilent, 2015)	Multi-scan (*CrysAlis PRO*; Agilent, 2015)
T_{min}, T_{max}	0.204, 1.000	0.206, 1.000
No. of measured, independent and observed [$I > 2\sigma(I)$] reflections	8833, 5033, 4580	9741, 5054, 4431
R_{int}	0.057	0.040
$(\sin\theta/\lambda)_{max}$ (Å^{-1})	0.628	0.628
Refinement		
$R[F^2 > 2\sigma(F^2)]$, $wR(F^2)$, S	0.043, 0.121, 1.06	0.039, 0.106, 1.02
No. of reflections	5033	5054
No. of parameters	273	290
H-atom treatment	H-atom parameters constrained	H-atom parameters constrained
$\Delta\rho_{max}$, $\Delta\rho_{min}$ (e Å^{-3})	1.75, −1.51	1.47, −1.58

Computer programs: *CrysAlis PRO* (Agilent, 2015), *SIR92* (Altomare *et al.*, 1993), *SHELXL2014* (Sheldrick, 2015), *ORTEP-3 for Windows* (Farrugia, 2012), *DIAMOND* (Brandenburg, 2006) and *publCIF* (Westrip, 2010).

yielding colourless slabs of (I). Yield: 52%, m.p. 364.6–365.4 K. Elemental analysis: calculated (%): C 57.8, H 5.8, N 2.6, S 11.9. Found (%): C 56.5, H 6.2, N 2.5, S 11.7. IR (KBr cm^{-1}): 1429 ν(C—N), 983 ν(C—S), 559 ν(Sn—C), 425 ν(Sn—S). ^{1}H NMR ($CDCl_3$): δ 7.41–7.77 (15H, C_6H_5); 3.38 (2H, N—CH_2); 3.42 (3H, N—CH_3); 2.21 (2H, N—CH_2CH_2); 1.75 (2H, N—$(CH_2)_2CH_2$); 1.59 (2H, N—$(CH_2)_3CH_2$); 1.34 (2H, N—$(CH_2)_4CH_2$); 0.92 (3H, hexyl—CH_3). ^{13}C NMR ($CDCl_3$): δ 196.04 (NCS_2); 128.52–142.53 (C-aromatic); 58.97 (NCH_2); 43.79 (NCH_3); 31.46 (N—CH_2CH_2); 26.98 [N—$(CH_2)_2CH_2$]; 26.39 [N—$(CH_2)_3CH_2$]; 22.6 [N—$CH_2)_4CH_2$]; 14.06 (hexyl—CH_3). ^{119}Sn NMR ($CDCl_3$): −187.56.

Synthesis of triphenyltin(IV) *N*-methyl-*N*-phenylethyldithiocarbamate (II): compound (II) was prepared in essentially the same manner as for (I) but using *N*-methyl-*N*-phenylethylamine (Aldrich; 1.45 ml, 10 mmol) in place of *N*-hexyl-*N*-methylamine. Recrystallization was achieved by dissolving the compound in a chloroform/ethanol mixture (1:2 *v*/*v*). Yield: 67%, m.p. 387.5–388.3 K. Elemental analysis: calculated (%): C 60.0, H 4.9, N 2.5, S 11.4. Found (%): C 57.9, H 5.3, N 2.8, S 11.2. IR (KBr cm^{-1}): 1452 ν(C—N), 977 ν(C—S), 502 ν(Sn—C), 488 ν(Sn—S). ^{1}H NMR ($CDCl_3$): δ 7.43–7.77 (15H, Sn—C_6H_5); 7.24–7.35 [5H, N$(CH_2)_2C_6H_5$]; 4.06 (2H, NCH_2); 3.36 (3H, NCH_3); 3.09 (2H, NCH_2CH_2). ^{13}C NMR ($CDCl_3$): δ 196.61 (NCS_2); 126.8–142.3 (C-aromatic); 60.25 (NCH_2); 44.59 (NCH_2CH_2); 33.12 (N—CH_3). ^{119}Sn NMR ($CDCl_3$) = −183.84.

7. Refinement

Crystal data, data collection and structure refinement details are summarized in Table 7. Carbon-bound H atoms were placed in calculated positions (C—H = 0.95–0.99 Å) and were included in the refinement in the riding-model approximation, with U_{iso}(H) set to 1.2–1.5U_{eq}(C). For (I), the maximum and minimum residual electron density peaks of 1.75 and 1.51 e Å^{-3}, respectively, are located 0.95 and 0.86 Å from the Sn atom. For (II), the maximum and minimum residual electron density peaks of 1.47 and 1.58 e Å^{-3}, respectively, are located 0.96 and 0.68 Å from the C11 and Sn atoms, respectively.

Acknowledgements

We gratefully acknowledge the School of Chemical Sciences and Food Technology, Universiti Kebangsaan Malaysia, for providing the essential laboratory facilities. We would also like to thank the laboratory assistants of the Faculty of Science and Technology, Universiti Kebangsaan Malaysia, for technical support received. Intensity data were collected in the University of Malaya's crystallographic laboratory.

Funding information

This work was supported by the Fundamental Research Grant Scheme (FRGS/2/2013/SKK10/UKM/02/1) awarded by the Ministry of Education (MOE).

References

Addison, A. W., Rao, T. N., Reedijk, J., van Rijn, J. & Verschoor, G. C. (1984). *J. Chem. Soc. Dalton Trans*. pp. 1349–1356.

Agilent (2015). *CrysAlis PRO*. Agilent Technologies Inc., Santa Clara, CA, USA.

Ali, S., Zia-ur-Rehman, Muneeb-ur-Rehman, Khan, I., Shah, S. N. A., Ali, R. F. Shaha, A., Badshah, A., Akbar, K. & Bélanger-Gariepy, F. (2014). *J. Coord. Chem*. **67**, 3414–3430.

Altomare, A., Cascarano, G., Giacovazzo, C. & Guagliardi, A. (1993). *J. Appl. Cryst.* **26**, 343–350.

Brandenburg, K. (2006). *DIAMOND*. Crystal Impact GbR, Bonn, Germany.

Buntine, M. A., Hall, V. J., Kosovel, F. J. & Tiekink, E. R. T. (1998). *J. Phys. Chem. A* **102**, 2472–2482.

Dance, I. & Scudder, M. (2009). *CrystEngComm*, **11**, 2233–2247.

Farrugia, L. J. (2012). *J. Appl. Cryst.* **45**, 849–854.

Green, M., Prince, P., Gardener, M. & Steed, J. (2004). *Adv. Mater*. **16**, 994–996.

Groom, C. R., Bruno, I. J., Lightfoot, M. P. & Ward, S. C. (2016). *Acta Cryst.* B**72**, 171–179.

Gupta, A. N., Kumar, V., Singh, V., Rajput, A., Prasad, L. B., Drew, M. G. B. & Singh, N. (2015). *J. Organomet. Chem*. **787**, 65–72.

Heard, P. J. (2005). *Prog. Inorg. Chem*. **53**, 1–69.

Hogarth, G. (2012). *Mini Rev. Med. Chem.* **12**, 1202–1215.

Hook, J. M., Linahan, B. M., Taylor, R. L., Tiekink, E. R. T., van Gorkom, L. & Webster, L. K. (1994). *Main Group Met. Chem*. **17**, 293–311.

Jotani, M. M., Tan, Y. S. & Tiekink, E. R. T. (2016). *Z. Kristallogr.* **231**, 403–413.

Lai, C. S. & Tiekink, E. R. T. (2007). *Z. Kristallogr*. **222**, 532–538.

McKinnon, J. J., Jayatilaka, D. & Spackman, M. A. (2007). *Chem. Commun*. pp. 3814–3816.

Mohamad, R., Awang, N., Jotani, M. M. & Tiekink, E. R. T. (2016). *Acta Cryst.* E**72**, 1130–1137.

Mohamad, R., Awang, N. & Kamaludin, N. F. (2016). *Res. J. Pharm. Biol. Chem. Sci*. **7**, 1920–1925.

Mohamad, R., Awang, N., Kamaludin, N. F. & Abu Bakar, N. F. (2016). *Res. J. Pharm. Biol. Chem. Sci*. **7**, 1269–1274.

Mohamad, R., Awang, N., Kamaludin, N. F., Jotani, M. M. & Tiekink, E. R. T. (2016). *Acta Cryst.* E**72**, 1480–1487.

Mohamad, R., Awang, N., Kamaludin, N. F., Jotani, M. M. & Tiekink, E. R. T. (2017). *Acta Cryst.* E**73**, 260–265.

Mohamad, R., Awang, N., Kamaludin, N. F., Jotani, M. M. & Tiekink, E. R. T. (2018). *Acta Cryst.* E**74**, 302–308.

Monteiro, O. C., Nogueira, H. I. S., Trindade, T. & Motevalli, M. (2001). *Chem. Mater*. **13**, 2103–2111.

Muthalib, A. F. A., Baba, I., Khaledi, H., Ali, H. M. & Tiekink, E. R. T. (2014). *Z. Kristallogr*. **229**, 39–46.

Park, J.-H., Afzaal, M., Kemmler, M., O'Brien, P., Otway, D. J., Raftery, J. & Waters, J. (2003). *J. Mater. Chem.* **13**, 1942–1949.

Ramasamy, K., Kuznetsov, V. L., Gopal, K., Malik, M. A., Raftery, J., Edwards, P. P. & O'Brien, P. (2013). *Chem. Mater*. **25**, 266–276.

Segovia, N., Crovetto, G., Lardelli, P. & Espigares, M. (2002). *J. Appl. Toxicol.* **22**, 353–357.

Sheldrick, G. M. (2015). *Acta Cryst.* C**71**, 3–8.

Spek, A. L. (2009). *Acta Cryst.* D**65**, 148–155.

Tiekink, E. R. T. (2008). *Appl. Organomet. Chem.* **22**, 533–550.

Tiekink, E. R. T., Hall, V. J. & Buntine, M. A. (1999). *Z. Kristallogr*. **214**, 124–134.

Westrip, S. P. (2010). *J. Appl. Cryst.* **43**, 920–925.